# Can polyoxometalates enhance the capacitance and energy density of activated carbon in organic electrolyte supercapacitors?

Jun-Jie Zhu[a], Raul Benages-Vilau[a], Pedro Gomez-Romero[a,b*]

[a] Catalan Institute of Nanoscience and Nanotechnology (ICN2), CSIC and BIST, Campus UAB, Bellaterra, 08193 Barcelona, Spain.

[b] Consejo Superior de Investigaciones Científicas (CSIC), Spain

* Corresponding author. E-mail address: pedro.gomez@icn2.cat (P. Gomez-Romero) Tel: +34 937373608, Fax: +34 936917640

ICN2, Campus UAB, 08193 Bellaterra (Barcelona) Spain

Highlights:

- Tetraethylammonium phosphotungstate (TEAPW12) and activated carbon (AC) were used to prepare a hybrid electrode able to outperform AC in a high-voltage organic electrolyte supercapacitor cell.
- The inorganic cluster undergoes multi-electron reactions integrated in the hybrid material, even in an aprotic organic electrolyte.
- Volumetric capacitance increases by ~36% with polyoxometalates hybridization without sacrificing voltage window.
- We are demonstrating for the first time the effective use of polyoxometalates in aprotic electrolyte supercapacitors.

Graphical abstract

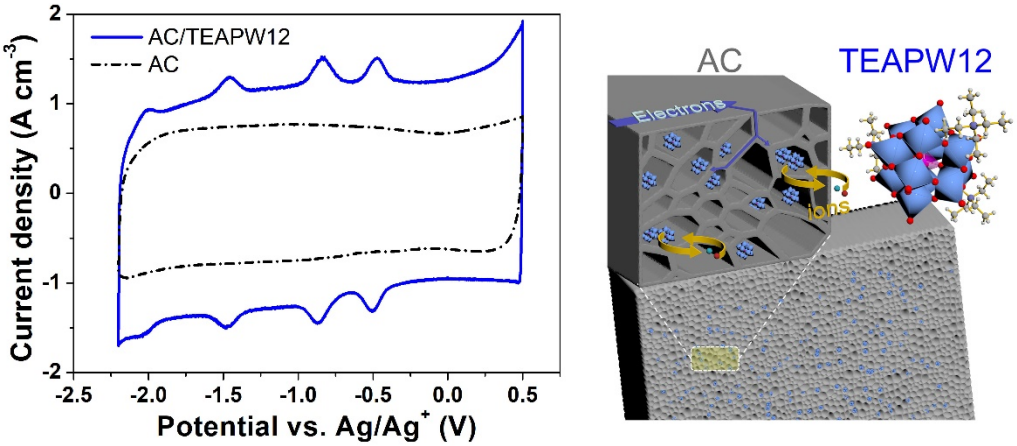

Abstract

Polyoxometalates (POMs) have been shown to work as faradaic additives to activated carbon (AC) in acidic aqueous electrolytes. Yet, their use in organic media allows not only for added capacity but also higher voltage. Here we show that the tetraethylammonium derivative of phosphotungstate $[PW_{12}O_{40}]^{3-}$ (PW12) can be homogeneously distributed throughout the pores of activated carbon (AC) in organic solvents such as N,N'-dimethylformamide (DMF) and demonstrate the use of this hybrid electrode material in an organic electrolyte (1 M TEABF4 in acetonitrile) supercapacitor. Our results show the efficient electroactivity of the PW12 cluster even in the absence of protons, providing a higher voltage than aqueous electrolytes and fast and reversible redox activity. The hybrid material shows a combination of double-layer (AC) and redox (PW12) capacities leading to an increase (36%) in volumetric capacitance with respect to pristine AC in the same organic electrolyte (1 M TEABF4 in acetonitrile). Remarkably, we were able to quantify this increase as coming predominantly from non-diffusion-limited processes thanks to the utterly dispersed nature of POMs. Moreover, the hybrid material delivers a good rate capability and excellent cycle stability (93% retention of the initial capacitance after 10,000 cycles). This study has a profound significance on improving capacitance of carbon-based materials in organic electrolytes.

Keywords: supercapacitor; polyoxometalate; organic electrolyte; hybrid electrode

# 1 Introduction

In the field of energy storage, supercapacitors stand out thanks to their high power density and long cycle life, but at the expense of low energy densities because charges are stored on the electrode-electrolyte interphase through electric double layer capacitance, (EDLC) and/or surface redox reactions (pseudo-capacitance)[1].

Combining high energy density, power density and long cycle life in a single device or material at low cost is the Holy Grail in energy storage. Active electrode materials determine the intrinsic energy density and power density of a certain device. Thus, most efforts have been made to explore novel electrode materials. A most promising approach is to design hybrid materials which combine both the merits of faradaic and non-faradaic materials to deliver both high energy density and power density[2-4]. The challenge lies here in the development of synergic active materials.

Carbon-based materials are non-faradaic materials used from the beginning in the development of supercapacitors (SCs), owing to their natural abundance, good electrical conductivity, and considerable capacitance related to their high specific surface area. Although carbon-based materials can deliver electric double layer capacitance, their capacitance is lower than those of transition metal oxides and conducting polymers whose capacitance arises from faradaic processes (pseudocapacitance)[5]. Numerous methods have

been utilized to furnish carbon-based materials with pseudocapacitive behavior, including heteroatom-doping or making composites[6].

Polyoxometalates (POMs) are transition metal oxide clusters typically 1 nm in size that can be easily anchored to other materials. POMs-based materials have been applied in various fields, including catalysis, electrochromic, magnetic, and energy storage[7, 8]. In a variety of energy storage devices, including supercapacitors[7-10], lithium ion batteries[11-13], flow cells[14, 15], fuel cells[16] we can see the great potential of POMs stemming from their multi-electron redox activities. And POMs not only can deliver superior energy but also they are structurally best suited to do it at a fast rate since all of their active moieties are at the surface of the cluster. Reduced graphene oxides[17], conducting polymers[8-12, 18-20], carbon nanotubes[21, 22], carbon nanopipes[23], micro-mesoporous carbons[24, 25] or activated carbons[26-28] have already been studied as the substrates for supporting POMs and all of them present some kind of enhanced capacitive performance, such as larger gravimetric specific capacitance[27], larger cell voltage window and/or longer cycle life[25, 26].

However, as it is well known, the redox chemistry of POMs is most effectively displayed in aqueous acidic media. This is undoubtedly the reason why the vast majority of the studies carried out for POMs in supercapacitors were made in (acidic) aqueous electrolytes. Under these conditions thermodynamics limits the potential window to 1.2 V due to water splitting. And

although some hybrid materials can extend the potential window up to 1.6 V[26], this value is still much lower than those attainable in organic electrolytes (2.7 - 3.5 V) or ionic liquids (ILs) (> 3.0 V)[3].

Since the energy density of a supercapacitor is proportional to the square of the operating voltage window for the cell, it comes as no surprise that organic or IL electrolytes are generally preferred for the design of high-energy systems. Yet, organic electrolytes are not problem-free, their greater viscosity, lower ionic conductivity which could produce a large amount of heat at high rate, and also the larger size of the ions dissolved tend to decrease their performance[29]. Thus, the capacitance of carbon-based materials is smaller in organic than in aqueous electrolytes. For instance, the specific capacitance of commercial activated carbon is around 100 F $g^{-1}$ in organic electrolytes but close to 200 F $g^{-1}$ in aqueous sulphuric acid[30]. Hybrid materials offer a path to break through this bottleneck as they introduce an alternative energy storage mechanism. Most achievements until now have resorted to inorganic salts of POMs (or their acids) to construct hybrid materials in order to boost capacitance in aqueous electrolytes. Recently, a few studies have been carried out on organic-inorganic POMs-based hybrid materials, but they are still applied for supercapacitors with aqueous electrolytes[31, 32], or for lithium ion batteries[33].

The question remains as to whether polyoxometalate clusters could be put to work as supercapacitor electrodes in organic electrolytes with the combined advantage of the superior voltage and increased capacity due to their redox

activity.

We report here for the first time such a system, based on a novel hybrid electrode material made of an organic phosphotungstate salt (tetraethylammonium phosphotungstate, TEAPW12) and activated carbon. As it will be shown, this material exhibits a combination of two charge storage mechanism: electrical double layer from activated carbon and faradaic process from TEAPW12, thanks to the anchoring of the organic phosphotungstate clusters onto the carbon microporous surface effectively leads to increased electrochemical behavior of the hybrid electrodes and to enhanced performance of symmetrical supercapacitor devices. Notably, this study explores an alternative strategy to boost the capacitance as well as the energy density of carbon-based materials in organic electrolytes.

# 2 Experimental

## 2.1 Materials and synthetic procedures

### 2.1.1 Materials

All raw chemicals were obtained commercially and used without additional purification. Tetraethylammonium chloride (≥98%), phosphotungstic acid hydrate, tetraethylammonium tetrafluoroborate (≥99%), dimethylformamide (anhydrous, ≥99.8%), acetonitrile (anhydrous, ≥99.8%), N-Methyl-2-pyrrolidone (≥ 99.5%) and poly(vinylidene fluoride) (average molecule weight ≈ 534000)

were purchased from Sigma Aldrich. Carbon black Super P (≥ 99%) was purchased from Alfa Aesar. Activated carbon DLC Super 30, specially produced for supercapacitor applications by Norit Chemical, was used. Nitrocellulose filter membranes (pore size=0.025 mm) purchased from MF-Milipore, Merck were used as separators.

### 2.1.2 Synthesis of TEAPW12

The organic-inorganic POM salt was synthesized through metathesis reaction in the light of the literature method[34]. Typically, 200 mL of a 20 mM aqueous solution of phosphotungstic acid was added to 200 mL of a 70 mM aqueous solution of tetraethylammonium chloride. A considerable amount of white precipitate appeared immediately. The suspension was kept stirring for 6 h, then filtered. The precipitate was washed with deionized water and dried overnight in air at 80 °C. Tetraethylammonium phosphotungstate ($[(C_2H_5)_4N)]_3PW_{12}O_{40}$) was obtained.

### 2.1.3 Synthesis of AC/TEAPW12

An AC suspension was prepared by sonicating AC (0.5 g) in DMF (100 ml) for 1 h. 6.6 g of TEAPW12 was added to the suspension. Then we kept it 5 h in a bath sonicator and stirred overnight. Finally, the sample was collected by filtration, and dried at 80 °C for 12 h in vacuum oven, around 0.63 g of the AC/TEAPW12 was obtained in each batch.

### 2.1.4 Synthesis of AC/HPW12.

For comparison, inorganic hybrid material (activated carbon with

phosphotungstic acid, named as AC/HPW12) was prepared following the previous literature methodology reported[26].

### 2.2 Material characterization

All the samples were dried at 120°C under vacuum overnight before the following material characterization.The thermal properties of the sample were studied by thermogravimetric analysis using NETZSCH-STA 449 F1 Jupiter thermal analysis system under air flow with a heating rate of 10 □C $min^{-1}$ from room temperature to 900 □C. The powder XRD patterns were collected on a PANalytical X'pert Pro-MRD diffractometer with Cu $K_\alpha$ radiation and PIXel detector. Volumetric $N_2$ sorption isotherms were collected at 77 K ($N_2$) using an ASAP 2020 HD (Micromeritics). Temperature was controlled by using a liquid nitrogen bath. Total pore volume ($V_{total}$) was calculated at $P/P_0$ = 0.95, and microporous volume ($V_{micro}$) was calculated using the Dubinin−Radushkevich equation. Pore size distribution was estimated using a density functional theory (DFT) model ($N_2$−cylindrical pores−oxide surface) implemented in the Microactive 4.00 software with a regularization factor of 0.01. High angle annular dark field scanning transmission electron microscopy (HAADF-STEM) images were taken on FEI Tecnai G2 F20 microscopy. Scanning electron microscopy images were taken on Quante 650 FEG microscopy.

### 2.3 Electrochemical characterization

The working electrodes were fabricated by mixing the active material, carbon black and poly(vinylidene fluoride) at a weight ratio of 85:5:10. Typically, the mixture was first formed as a slurry by adding a few drops of N-methyl-2-pyrrolidinone, then coated onto aluminum foil (>99%, with the thickness of 0.05 mm) with doctor-blade method (RK PrintCoat, with the gap of 60 μm) , and dried under vacuum at 120 °C for 12 h. The loading mass of each electrode is in the range of 1.5-2 mg $cm^{-2}$. Three-way stainless steel Swagelok® cells were used to characterize the materials in three-electrode configuration. $Ag/Ag^{+}$ (0.01 M $AgNO_3$) was used as reference electrode. An electrode loaded with double weight of the same active material was used as counter electrode. Symmetrical supercapacitors formed by two identical electrodes were assembled in CR2032 coin cells with a coin-cell crimper (TMAXCN). All the electrodes were cut in the diameter of 14 mm and pressed at 3 MPa before assembling. 1 M tetraethylammonium tetrafluoroborate (TEABF4) in acetonitrile was used as the electrolyte. All the cells were assembled in an argon-filled glovebox (Jacomex GP with $O_2$ < 5 ppm and $H_2O$ < 5 ppm). Cyclic voltammetry (CV) was performed in a three-electrode configuration at the various scan rates to investigate the capacitive behavior of individual electrodes. Cyclic polarization (CP) and galvanostatic charge-discharge (GCD) was performed in two-electrode cell to evaluate the capacitive performance in devices, and cycling stability. All the electrochemical tests were conducted on Biologic VMP3 multi-channel potentiostat.

## 3 Result and discussion

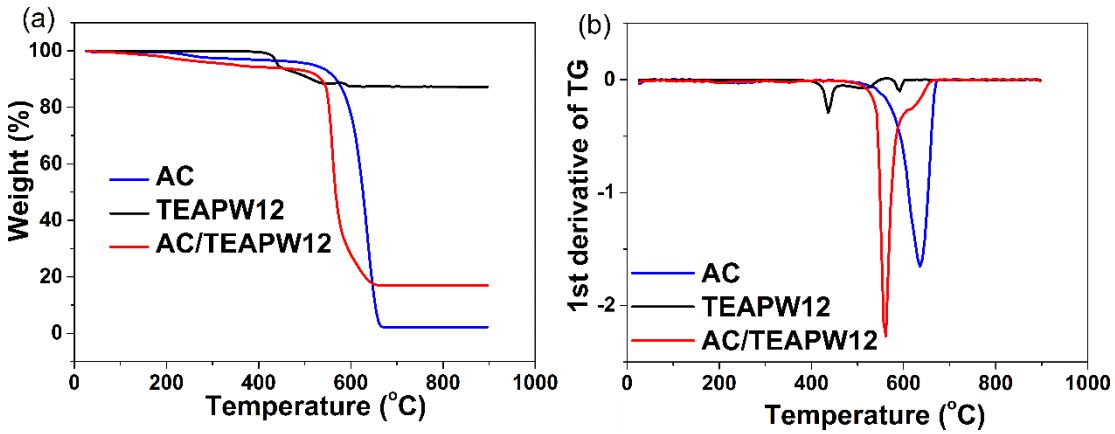


Fig. 1. (a) Thermogravimetric and (b) corresponding derivative (dw/dT) curves of AC/TEAPW12, TEAPW12 and pristine AC with the heating rate of 10 °C $min^{-1}$ under dry air flow.

Fig. 1 presents the thermogravimetric curves and their corresponding derivative (dw/dT) curves of AC/TEAPW12, TEAPW12 and pristine AC. The pristine AC undergoes a slight weight loss (3.2%) before 400 °C, corresponding to the removal of adsorbates. Subsequently, a drastic drop of weight refers to the combustion of carbon in air. Finally, 2.18% of its initial weight remains as ashes. On its dw/dT curve, only one sharp peak can be discerned, corresponding to the combustion. Pure TEAPW12 exhibits a more complicated decomposition process. Its weight suffers a negligible loss (0.39%) when heating up to 400 °C, indicating that there is scarcely any crystal water in this salt (0.7 $H_2O$ per TEAPW12 molecule). Afterwards, a remarkable weight loss, ranging from 400 °C to 600 °C, can be discerned, which should be assigned to the decomposition of tetraethylammonium moieties. The weight loss in this stage is 12.2%, in good agreement with the expected proportion of tetraethylammonium moieties (11.9%) in TEAPW12. The dw/dT curve presents

three peaks, revealing that in this stage the decomposition involves several steps. The step-by-step decomposition process of tetraethylammonium has been verified in thermal decomposition study on tetraethylammonium in zeolites[35]. At the end, the weight stays relatively stable above 650 °C. Concerning the decomposition of phosphotungstate, Chiang et .al.[36], reported that after 360°C, anhydrous phosphotungstate starts to transform into a new tetragonal phase, a light-green coloured phosphotungstate of empirical formula $P_2O_5 \cdot 24WO_3$ which is stable up to 1000 °C, and then decomposes gradually and some phosphorus oxides vaporize. In our case, a residue of $P_2O_5 \cdot 24WO_3$ would account for 87.2 wt.% of TEAPW12, in very good agreement with the experimentally found residual weight (87.3% at 800ºC). The thermogravimetric curve of AC/TEAPW12 is similar to that of pristine AC, as AC makes up most of the hybrid material. On the other hand, the temperature of decomposition of activated carbon is ca. 50 ºC lower in the presence of phosphotungstate clusters (PW12), most likely due to the catalytic activity of this cluster at high temperature.

Finally, the residual weight after AC/TEAPW12 decomposition is 17 %, from which we can estimate that the hybrid material contains a 17.5 wt.% of TEAPW12.

Microstructural analyses were performed by a variety of methods in order to confirm the dispersion of TEAPW12 on AC. SEM images of the pristine AC (Fig.S1a) and the hybrid material AC/TEAPW12 (Fig.S1b) present no apparent

difference, both exhibiting a blocky morphology. No apparent agglomeration nor crystallization of TEAPW12 can be detected in SEM images. On the other hand, the energy dispersive X-ray (EDX) spectra (see Fig. S1d) show a definitive difference between AC and the hybrid. The EDX spectrum of AC/TEAPW12 presents one extra peak at 1.78 eV, corresponding to W.

In order to study the distribution characteristics of TEAPW12, samples were observed under scanning transmission electron microscopy in high angle annular dark field (HAADF-STEM). HAADF-STEM images show the difference apparently. The image of AC (Fig. 2a) reveals its inhomogeneous nature. Plenty of micropores (pore size < 2 nm) and mesopores (pore size from 2 to 50 nm), corresponding to the dark areas in the image, can be discerned. In contrast, the image of AC/TEAPW12 (Fig. 2b) does not present similar dark area, but uniformly-distributed sparkly dots, which correspond to tungsten in TEAPW12 (confirmed by line scan of EDX, see Fig. S2b). The disappearance of the dark area in AC/TEAPW12 can be explained in two ways. Firstly, the TEAPW12 molecules in the pores leads to a slight fall of both surface area and pore volume[25]; secondly, the strong contrast between sparkly dots and dark pore makes the dark area less visible.

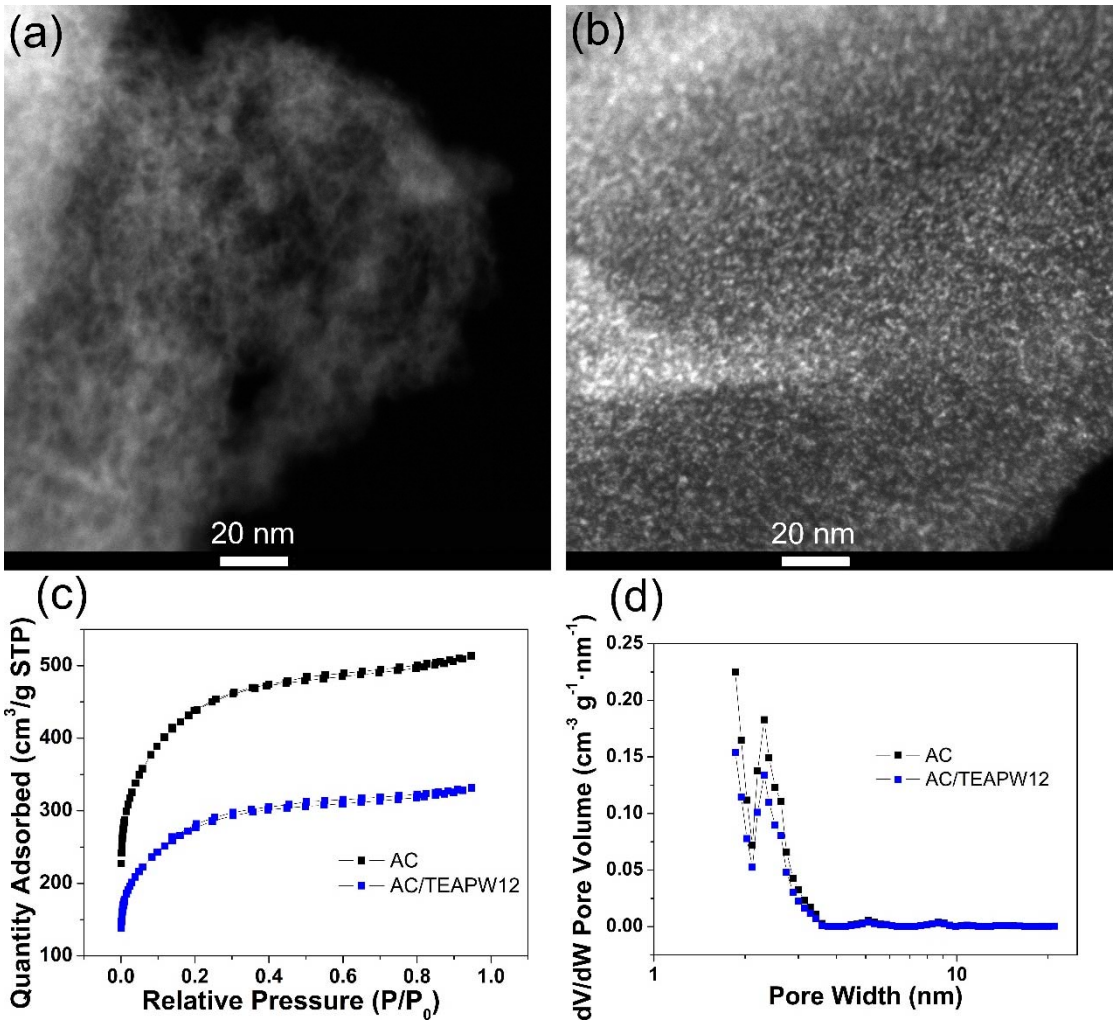


Fig. 2. HAADF-STEM images of (a) AC and (b) AC/TEAPW12. (c) $N_2$ sorption isotherms and (d) Pore size distribution curves of AC and AC/TEAPW12.

Table 1 Porosity properties of samples AC and AC/TEAPW12

| Sample | $S_{BET}$[a] ($m^2$ $g^{-1}$) | $V_{Total}$[b] ($cm^3$ $g^{-1}$) | $V_{Micro}$[c] ($cm^3$ $g^{-1}$) |
|---|---|---|---|
| AC | 1603 | 0.712 | 0.344 |
| AC/TEAPW12[d] | 1007 | 0.453 | 0.191 |
| AC/TEAPW12[e] | 1220 | 0.549 | 0.232 |

a, Specific surface area determined according to BET method. b, Total pore volume. c. Micropore volume. d, all the data in this line are normalized by the total weight. e, all the data in this line are normalized by the weight of AC.

Even though TEAPW12 accounts for ca. 17.5 wt% in AC/TEAPW12, the XRD pattern of AC/TEAPW12 (see Fig. S2c) only presents a broad bump,

similar to that found for pristine AC. This confirms that TEAPW12 clusters spread on the AC substrate homogeneously in the form of isolated clusters instead of well-crystallized extended solid particles.

The influence of the absorption of TEAPW12 on the porous properties of AC was evaluated by volumetric $N_2$ sorption experiments. Fig. 2c shows the $N_2$ sorption isotherms of AC and AC/TEAPW12. Both of them can be classified as Type I isotherm according to the IUPAC classification, revealing their microporous nature. Moreover, these two samples share the same pore size distribution, in which most pores fall within or close to the micropore range. The similar $N_2$ sorption isotherms and pore size distribution curves confirm that absorption of TEAPW12 on AC does not affect significantly its porous nature. However, the specific surface area and micropore volume (Table 1) are reduced from 1603 $m^2\ g^{-1}$ (AC) to 1007 $m^2\ g^{-1}$ (AC/TEAPW12,) and from 0.344 $cm^3\ g^{-1}$ (AC) to 0.191 $cm^3\ g^{-1}$ (AC/TEAPW12), respectively. In principle this should be expected since the PW12 cluster is formed by heavy metals. However, the same trend is detected when normalizing per mass of AC (Table 1). Furthermore, the drop of micropore volume (-44.5%) is larger than that of specific surface area (-37.2%) or total pore volume (-36.3%). This leads us to speculate that the TEAPW12 clusters are mainly absorbed in the micropores of AC.

Based on the weight percentage, specific surface area and micropore volume, we can estimate if the surface of AC is large enough to spread

TEAPW12 in a single layer and the micropore of AC is enough to accommodate all TEAPW12 clusters. We assume the projected area and occupied volume per TEAPW12 cluster is 1 $nm^2$ and 1 $nm^3$, respectively. The area to spread TEAPW12 cluster in monolayer is 32.2 $m^2$ per gram of AC/TEAPW12. This is much lower than its specific surface area. The volume to accommodate TEAPW12 in 1 g of AC/TEAPW12 is 0.03 $cm^3$, much less than the total micropore volume. Therefore, AC can provide enough area to spread TEAPW12 clusters as monolayer, and enough micropores to accommodate all the TEAPW12 clusters.

Since TEAPW12 is composed of twelve $WO_6$ octahedra, all of them on the surface of the cluster and exposed to the electrolyte, the adsorption of these clusters on carbon affords the possibility to harness their faradaic redox activity without the sluggish ion diffusion found in extended phases. Besides, in this case AC acts not only as the substrate for immobilizing POM clusters, but also as a conducting matrix facilitating electron transport and transfer during the faradaic process.

Fig. 3a presents the cyclic voltammograms of AC and AC/TEAPW12 at the scan rate of 20 mV $s^{-1}$. Its *y* axis is the current normalized per volume of electrode. The CV of AC is nearly a rectangle, indicating ideal capacitive behavior. On the other hand, four pairs of redox peaks, which have the $E_{1/2}$ of -0.492, -0.851, -1.469 and -2.02 V vs. $Ag/Ag^+$ ($E_{1/2}$ refers to the mid-point potential between oxidation peak and reduction peak), can be distinguished on

the CV of AC/TEAPW12. In the previous studies on phosphotunsgtic acid/carbon-based hybrid materials in acidic electrolytes, only three redox pairs could be discerned and the most negative one which involved two electrons was pH-dependent[26]. It should be stressed that protons are crucial in aqueous electrolytes for keeping the overall charge of the POM clusters at a low 3-/4- by concomitant protonation during reduction. Thus, in the absence of protons in the present organic electrolytes, we consider that the TEA counterions must fulfill a similar role most likely through the formation of ion pairs, as it has been previously reported in other organic solvents with a variety of cations[37-39].

Furthermore, we postulate that due to the absence of protons in the organic electrolyte and the formation of ion pairs with the TEA cations, the most negative pH-dependent redox wave has split in two. Indeed, this behavior is similar to a previously reported splitting in organic media[40].

We have estimated the contribution from TEAPW12 to the total stored charge in AC/TEAPW12 electrode with the assumption that hybridization does not affect the capacitive performance of AC (details are presented in supporting information S5). We find all the TEAPW12 clusters are utilized, which would account for 93.8% for the increased stored charge. Apart from the contribution from TEAPW12, the remaining slight increase could be due to the modification of the structure or the changed surface state of activated carbon after the hybridization. In other words, we can now state that the expected theoretical

contribution of POM to reversible charge storage and the measured charge are compatible with all the 17.5 wt% of POM in the hybrid reversibly exchanging four electrons per cluster

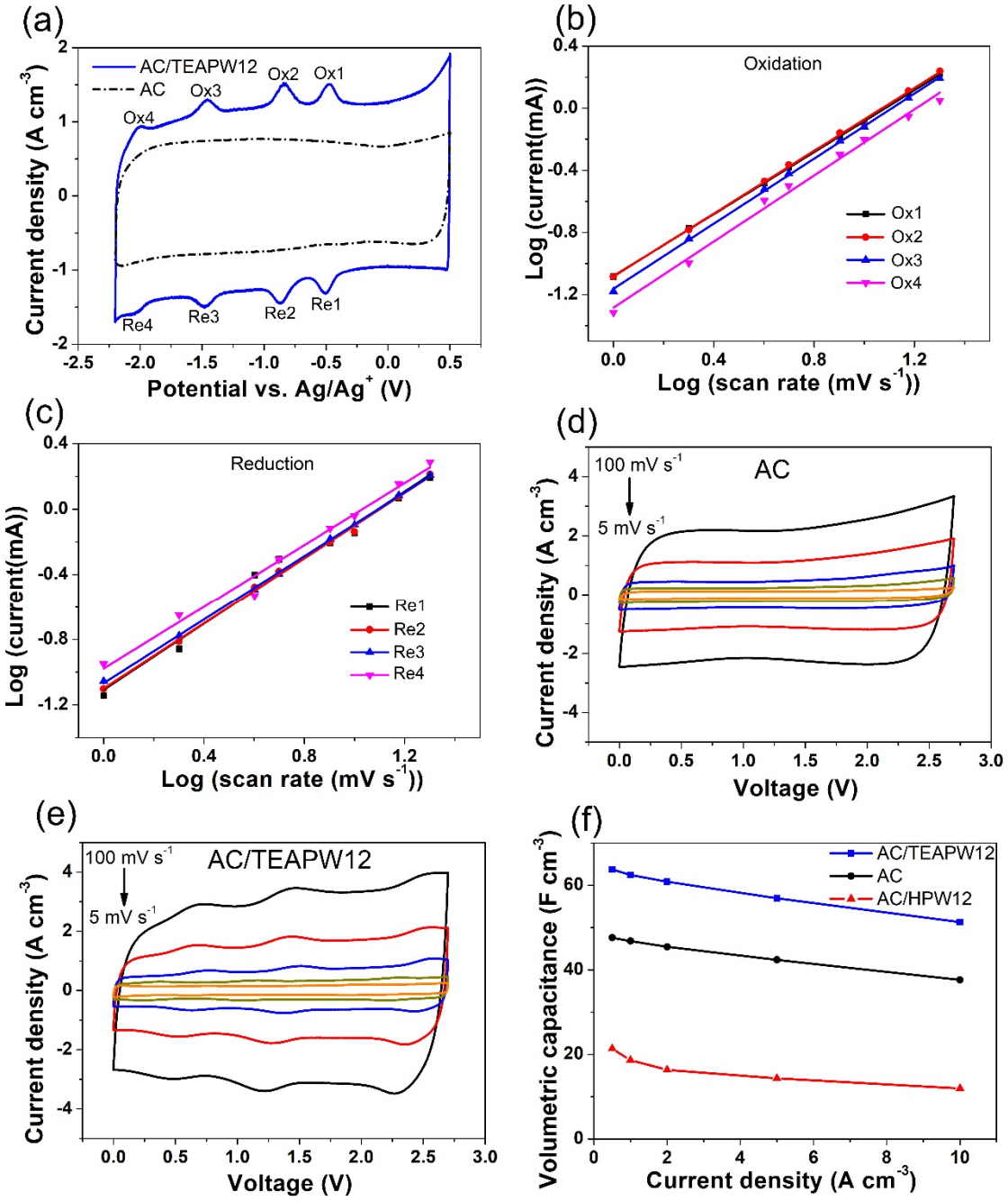


Fig. 3. (a) Cyclic voltammograms of AC and AC/TEAPW12 at 20 mV $s^{-1}$ in three-electrode configuration, the *y* axis is the current normalized per volume of electrode. b-value determination for (b) oxidation peaks and (c) reduction peaks of CVs of AC/TEAPW12. Cyclic polarization curves of (d) AC and (e) AC/TEAPW12 in two-electrode cell at 5, 10, 20, 50 and 100 mV $s^{-1}$. (f) Volumetric capacitance of AC, AC/TEAPW12 and AC/HPW12 at various current densities. In all cases the electrolyte

was 1M TEABF4 in $CH_3CN$.

On the other hand, we note that the voltage specific activity associated to these redox processes shows in the CVs (Fig 3a) as relatively weak peaks, whereas a rectangular-shaped capacitive component seems to dominate. This is expected for the purely capacitive AC but somewhat surprising for the hybrid.

Thus, the charge-storage mechanism was further analyzed by estimating the surface capacitive and ion-diffusion controlled charge contribution to the total charges stored by AC/TEAPW12 electrodes. Since the redox reaction of TEAPW12 in TEABF4/acetonitrile involves formation of ion pairs, it could be limited by the slow diffusion of cations. For this analysis, the CV curves at various scan rates were measured and presented in Fig. S3a. The dependence of the current response on the scan rate can provide insights into the charge-storage mechanism according to Eq1[41]:

$$i = av^b \qquad \text{Eq1}$$

where *i* is the maximum peak current obtained at a specific scan rate *v*, and *a* and *b* are adjustable parameters. The current response of a linear dependence on scan rate (b = 1) usually means charge is stored by a fast response mechanism, such as surface capacitive mechanism and redox reactions which could perform at fast rate[31]. Otherwise, if any slow diffusion of ion or electron transfer limits the reaction, the dependence could deviate from linearity (b < 1). The following equation

$$log\, i = log\, a + b\, log\, v \qquad \text{Eq2}$$

can be derived from Eq1, so that the value of *b* for different potentials can be determined from the slope of the straight line of log *i* vs log *v*, as shown in Fig. 3b and Fig. 3c. Herein, we mainly evaluate the *b* value for the four pairs of redox peaks. Table 2 presents the fitting results. All $R^2$ values are close to 1, confirming proper fittings. More importantly, all the *b* values are very close to 1, within experimental error, which means that the charge-storage process is not limited by any diffusion of cations nor interfacial electron transfer, even around the redox potentials characteristic of the PW12 clusters. At first sight this might seem surprising for redox-active clusters such as POMs. Indeed, bulky POM-containing materials frequently exhibit ion-diffusion-controlled responses as detected from their CVs[13, 42]. In our case, however, the fast current response ascertained must be associated to the fact that all electroactive moieties (WO6) are directly available at the electrode-electrolyte interface for electron injection with simultaneous ion-pair formation. This is only possible by the proper dispersion and homogeneous distribution of POM clusters at the molecular nanoscale level, and it is at the heart of the working of these electrodes at fast rates, effectively working as pseudocapacitors. A similar instance of this behaviour was reported by Ma et al. in the study on silicotungstate in an open 3D framework of [Cu(1,4-bis(triazol-1-ylmethyl)benzene)$_4$][31]. Finally, it could be noted that a size effect on charge-storage mechanism is also observed for other common nanoparticulate redox active materials, such as $TiO_2$, $LiCoO_2$ and $V_2O_5$[41]. Thus, our result is perfectly compatible with PW12 clusters being

distributed on AC substrate at a molecular level.

Table 2 Values of *b* (eqs. 1 and 2) and regression coefficients ($R^2$) derived from fitting current of reduction peaks (Re) and oxidation peaks (Ox) at various scan rates.

| | Re1 | Ox1 | Re2 | Ox2 | Re3 | Ox3 | Re4 | Ox4 |
|---|---|---|---|---|---|---|---|---|
| b | 0.99 | 1.0 | 1.0 | 1.0 | 1.0 | 0.98 | 1.0 | 0.95 |
| $R^2$ | 0.9996 | 0.9787 | 0.999 | 0.9978 | 0.9994 | 0.9996 | 0.9924 | 0.9819 |

To evaluate the capacitive performance of the hybrid materials in real devices, symmetrical capacitors were assembled in coin cells. The shape of cyclic polarization curves of the AC symmetric cell (Fig. 3d) is ideally rectangular confirming its capacitance is mainly derived from a double layer mechanism. In contrast, the CP curves of AC/TEAPW12 (Fig. 3e) symmetric cell present three pairs of waves added to the rectangular shape, revealing its hybrid nature. The volumetric capacitance of AC/TEAPW12 derived from the CP at 5 mV $s^{-1}$ is 66 F $cm^{-3}$ (Fig. S3b), 35% higher than that of AC. When the scan rates rise to 100 mV $s^{-1}$, the contours of the waves remain, verifying the good rate capability of the faradaic process. 93% of the capacitance at 5 mV $s^{-1}$ remains when the scan rate rises to 100 mV $s^{-1}$, indicating the excellent rate capability of AC/TEAPW12. This should be assigned to the homogeneous distribution of TEAPW12 on AC as we have confirmed in HAADF-STEM images, to the electronic conductivity provided by the carbon matrix and to the direct contact of all the electroactive centers with the electrolyte which precludes the

need of any bulk ion diffusion.

The CV of an AC/TEAPW12 electrode in a three-electrode cell shows four pairs of redox waves as discussed above. On the other hand, the CP curves of two identical AC/TEAPW12 electrodes in two-electrode cell shows just three pairs of waves. This is perfectly compatible with the CV and it can be explained by the fact that the initial potential of each of the two identical AC/TEAPW12 electrodes is -0.7 V vs. $Ag/Ag^{+}$, which is nearly in between the first two redox pairs of the CV (Ox1/Re1 and Ox2/Re2). Once the symmetric supercapacitor begins to charge, both the positive and negative electrode suffer redox reactions simultaneously (the positive Ox1, the negative Re2) thus leading to the first wave on the CP curves of the symmetric supercapacitor. After this, only the negative electrode will suffer redox reactions corresponding to Ox3/Re3 and Ox4/Re4 and leading to the other two pairs of waves in the CP curves. The variation of the potential of both positive and negative electrodes, as well as the symmetric capacitor voltage during GCD can be seen in Fig. S3c. Moreover, symmetrical supercapacitor based on inorganic hybrid material (AC/HPW12) were also characterized for comparison. The CP curves of AC/HPW12 (Fig. S3d) also exhibit polarization waves deriving from redox activity. However, both their specific capacitance and rate performance were poorer than for AC/TEAPW12 devices.

Galvanostatic charge-discharge was tested to evaluate the performance of symmetric supercapacitor under working conditions. The GCD curves are

presented in Fig. S4a and b. Fig. 3f presents the volumetric capacitance at different current densities. AC/TEAPW12 exhibits a considerably higher volumetric capacitance, with a gain of ca. 36% enhancement, compared to AC. The improvement of capacitance can be attributed to the added activity of TEAPW12. It is currently understood that the origin of pseudocapacitance lies on the fast reversible faradaic processes taking place on the surface or near-surface of active phases[43]. In our case all the electroactive centers of all the clusters are surface-active. Therefore, the homogeneous distribution of TEAPW12 provides numerous active sites on surface, allowing for the optimal harnessing of the clusters redox activity. In contrast, the capacitance of AC/HPW12 is lower, contrary to the trend in aqueous electrolytes[26]. What is the reason for the drastic underperformance of $H_3PW_{12}O_{40}$ in the present organic electrolyte? This different behavior must be associated to different reaction mechanisms. For instance, the deprotonation of acidic PW12 must be hindered in acetonitrile, probably due to the lack of a proton-accepting base such as $H_2O$. Thus, in addition to the important effect of cations in POM chemistry, we believe this underperfomance could be due to the dispersion of a solid acid such as $H_3PW_{12}O_{40}$ in a non-aqueous electrolyte impeding the very effective Grotthuss mechamism taking place in protonated water.

Thus, contrary to the acidic derivative, TEAPW12 can effectively carry on the redox reaction in organic electrolytes without protons and contribute its redox activity to the total capacitance of the hybrid material. Gravimetric specific

capacitance is also characterized by galvanostatic charge-discharge technique (Fig S4c). AC/TEAPW12 exhibits nearly equivalent gravimetric specific capacitance with respect to AC in the whole range (around 82 F $g^{-1}$ at 0.5 A $g^{-1}$ and around 67 F $g^{-1}$ at 20 A $g^{-1}$). This is not surprising given the very large molecular weight of TEAPW12 (ca. 3270 g/mol), which, when normalizing per mass, compensates for the increased capacitance provided by the cluster. On the other hand, when the key is compactness, that is, when volume normalization prevails, the AC/TEAPW12 electrode is a winner, since compact, 1 nm PW12 molecular clusters are directly attached to the porous surface of AC with no addition to the volume of the carbon material.

We tested the rate performance of our materials by measuring capacitances as a function of discharge current density (Fig. 3d). It should be noted that AC/TEAPW12 supercapacitors are superior to AC in the whole range. Furthermore, the drop in capacitance at fast rates is relatively small. Thus, by increasing the current density from 0.5 A $cm^{-3}$ to 10 A $cm^{-3}$ the capacitance values drop to 80.1 % (AC/TEAPW12) and 79.9 % (AC), suggesting good rate capability. As both the AC and hybrid electrodes are mainly composed of activated carbon (85 wt. % for AC electrode, 66 wt.% for AC/TEAPW12 electrode with carbon black and poly(vinylidene fluoride) accounting for 15%) and since the activated carbon acts as both substrate and conductor for TEAPW12, it is reasonable to ascribe the limitation on the rate capability to activated carbon.

In addition, the energy and power densities of these supercapacitors are compared and presented in the Ragone plot (see Fig. S4d). The maximum energy density for AC/TEAPW12 cell is found to be 16 mWh $cm^{-3}$ at the power density of 1.35 W $cm^{-3}$, which is 36% higher than that of AC. The energy density of AC/TEAPW12 outperforms that of AC in the same power density range thanks to the improved volumetric capacitance and the superior cell voltage. Moreover, with respect to recently reported activated carbon-based supercapacitors, the AC/TEAPW12 surpass those both in aqueous electrolytes and organic electrolytes[44-47]. This behavior is similar to some previously reported materials made from activated carbon with redox active additives[48] or heteroatom doping[49, 50]. Yet, it represents an alternative way to introduce pseudocapacitance without doping the carbon or adding redox active species to the electrolyte (which normally leads to faster self-discharge), just by adsorbing electroactive molecular clusters onto AC.

Finally, we are presenting our cycle stability. Fig. 4a shows the retention of the initial capacitance values for AC and AC/TEAPW12 symmetric capacitors as a function of the cycle number. The capacitance of AC/TEAPW12 increases a little bit due to the activation process in the first cycles, which is normal for materials with pseudocapacitance[51]. In contrast, the capacitance of AC decreases from the beginning at a low but steady rate. After 10000 cycles, the retention of both cells is higher than 91%, and owing to the increase of capacitance at the first stage, the retention of AC/TEAPW12 is even higher

(93%). Fig. 4b–e show the morphologies of AC and AC/TEAPW12 electrodes before and after cycling. Even after 10000 cycles, both AC and AC/TEAPW12 electrodes present no apparent difference except for a small amount of electrolyte residue. HAADF-STEM was performed to investigate the effective anchoring of TEAPW12 on AC after cycling (Fig. 4f). The bright dots associated to PW12 clusters spread on the AC substrate uniformly, demonstrating that even after 10000 charge-discharge cycles and acetonitrile washing, PW12 clusters are still anchored on AC. EDX spectra of cycled and washed AC/TEAPW12 is present in Fig. S6b. The existence of W is clearly verified. Moreover, a coin cell with the AC electrodes and the used electrolytes collected from AC/TEAPW12 cell is assembled to testify that TEAPW12 has not been dissolved in the electrolyte, at least not enough to present any redox waves (Fig. S6a). Thus, we could conclude that TEAPW12 clusters are anchoring on AC tightly, even after 10000 cycles and acetonitrile washing. This should be attributed to the fact that the PW12 are mainly anchored in the micropores of similar size. Thanks to the stability of AC substrate and the tight anchoring of TEAPW12, the hybrid electrodes could deliver an excellent cycle stability in organic electrolytes

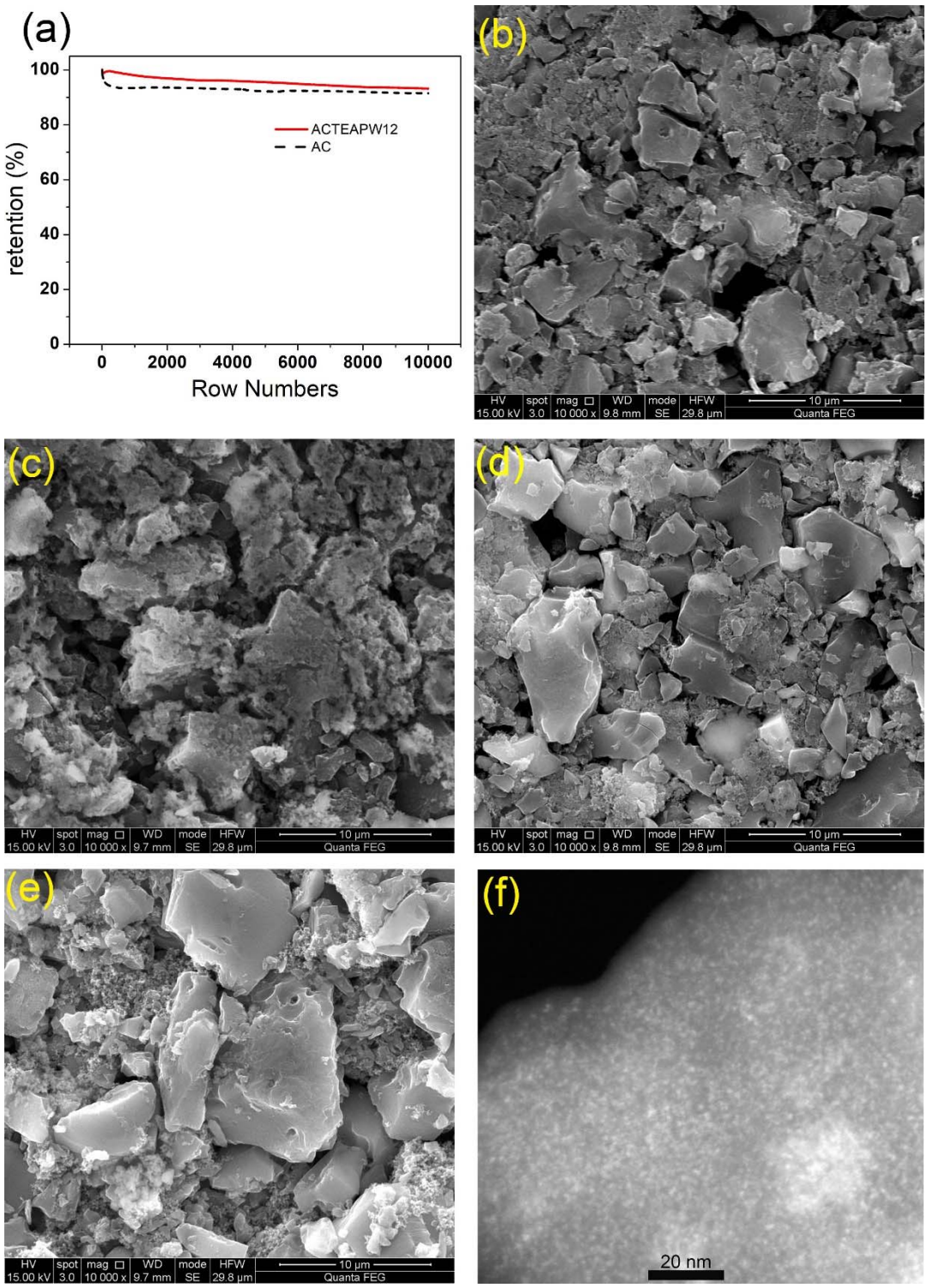


Fig. 4. (a) Capacitance retention upon cycling for AC and AC/TEAPW12 at the current density of 8 A $g^{-1}$. SEM images of AC (b) before and (c) after cycling. SEM images of AC/TEAPW12 (d) before and (e) after cycling. (f) HAADF-STEM images of AC/TEAPW12 electrode washed with acetonitrile after 10,000 cycles.

# 4 Conclusion

In this work an organic-inorganic polyoxometalate salt (TEAPW12) was exploited to hybridize with activated carbon in a facile way in order to enhance the capacitive performance of activated carbon in organic electrolytes. The as-prepared hybrid material was characterized by TGA and HAADF-STEM, showing a homogeneous distribution of TEAPW12 clusters anchored in the pores of AC with a final mass percentage of 17.5 % of TEAPW12. The hybrid material was tested in a conventional organic electrolyte (1 M TEABF4 in acetonitrile) in both three-electrode cell and two-electrode cell(as symmetric supercapacitors). The organic-inorganic hybrid material exhibits superior performance as compared with the parent AC supercapacitor system. But also, very remarkably, in this organic media the AC/TEAPW12 hybrid electrode shows better performance than the hybrid material based on the phosphotungstic acid derivative (AC/HPW12). Our work shows that the fast reversible redox reactions of PW12 can proceed in the absence of protons, provided by the use of a suitable salt. Owing to the faradaic process of TEAPW12 in the organic electrolyte, the symmetrical capacitors of the hybrid material show an increment of 36% in volumetric capacitance with respect to that of AC, good rate capability and good cycle stability (93% of initial capacitance retained after 10000 cycles). Therefore, applying organic POMs salts, instead of inorganic POMs acids or salts, to construct hybrid materials has been proven to be an effective route to enhance the capacitance of carbon-based materials in organic electrolytes.

*Acknowledgements*

Partial funding from Ministry of Science, Innovation and Universities (MCIU), the State Research Agency (AEI) and the European Regional Development Fund (FEDER) (grant RTI2018-099826-B-I00) and AGAUR (2017 SGR 00870)

are gratefully acknowledged. ICN2 is funded by the CERCA programme / Generalitat de Catalunya, and it is supported by the Severo Ochoa Centres of Excellence programme, funded by the Spanish Research Agency (AEI, grant no. SEV-2017-0706). J.J Z. acknowledges his scholarship (No. 201806370211) under China Scholarship Council. This work has been carried out within the framework of doctoral program (PhD) of Material Science (Department of Physics) of Universitat Autònoma de Barcelona (UAB).

## Reference


[1] D.P. Dubal, N.R. Chodankar, D.H. Kim, P. Gomez-Romero, Chem Soc Rev, 47 (2018) 2065-2129. https://doi.org/10.1039/c7cs00505a

[2] C. Choi, D.S. Ashby, D.M. Butts, R.H. DeBlock, Q. Wei, J. Lau, B. Dunn, Nature Reviews Materials, (2019). https://doi.org/10.1038/s41578-019-0142-z

[3] Z. Lin, E. Goikolea, A. Balducci, K. Naoi, P.L. Taberna, M. Salanne, G. Yushin, P. Simon, Materials Today, 21 (2018) 419-436. https://doi.org/10.1016/j.mattod.2018.01.035

[4] S. Li, L.L. Yu, Y.T. Shi, J. Fan, R.B. Li, G.D. Fan, W.L. Xu, J.T. Zhao, ACS Appl Mater Interfaces, 11 (2019) 10178-10188. https://doi.org/10.1021/acsami.8b21063

[5] X. Chen, R. Paul, L. Dai, National Science Review, 4 (2017) 453-489. https://doi.org/10.1093/nsr/nwx009

[6] F. Beguin, V. Presser, A. Balducci, E. Frackowiak, Adv Mater, 26 (2014) 2219-2251, 2283. https://doi.org/10.1002/adma.201304137

[7] M. Skunik-Nuckowska, S. Dyjak, K. Grzejszczyk, N.H. Wisinska, F. Beguin, P.J. Kulesza, Electrochimica Acta, 282 (2018) 533-543. https://doi.org/10.1016/j.electacta.2018.06.070

[8] D.P. Dubal, B. Ballesteros, A.A. Mohite, P. Gomez-Romero, ChemSusChem, 10 (2017) 731-737. https://doi.org/10.1002/cssc.201601610

[9] P. Gómez-Romero, M. Chojak, K. Cuentas-Gallegos, J.A. Asensio, P.J. Kulesza, N. Casañ-Pastor, M. Lira-Cantú, Electrochemistry Communications, 5 (2003) 149-153. https://doi.org/10.1016/S1388-2481(03)00010-9

[10] A.K. Cuentas‐Gallegos, M. Lira‐Cantú, N. Casañ‐Pastor, P. Gómez‐Romero, Advanced Functional Materials, 15 (2005) 1125-1133. https://doi.org/10.1002/adfm.200400326

[11] P. Gómez‐Romero, M. Lira‐Cantú, Advanced Materials, 9 (1997) 144-147. https://doi.org/10.1002/adma.19970090210

[12] M. Lira-Cantú, P. Gómez-Romero, Chemistry of materials, 10 (1998) 698-704. https://doi.org/10.1021/cm970107u

[13] S.-C. Huang, C.-C. Lin, C.-W. Hu, Y.-F. Liao, T.-Y. Chen, H.-Y. Chen, Journal of Power Sources, 435 (2019) 226702. https://doi.org/10.1016/j.jpowsour.2019.226702

[14] J. Friedl, M.V. Holland-Cunz, F. Cording, F.L. Pfanschilling, C. Wills, W. McFarlane, B. Schricker, R. Fleck, H. Wolfschmidt, U. Stimming, Energy & Environmental Science, 11 (2018) 3010-3018. https://doi.org/10.1039/c8ee00422f

[15] D.P. Dubal, D. Rueda-Garcia, C. Marchante, R. Benages, P. Gomez-Romero, The Chemical Record, 18 (2018) 1076-1084. https://doi.org/10.1002/tcr.201700116

[16] N.L.O. Gunn, D.B. Ward, C. Menelaou, M.A. Herbert, T.J. Davies, Journal of Power Sources, 348 (2017) 107-117. https://doi.org/10.1016/j.jpowsour.2017.02.048

[17] F.C. Shen, Y.R. Wang, S.L. Li, J. Liu, L.Z. Dong, T. Wei, Y.C. Cui, X.L. Wu, Y. Xu, Y.Q. Lan, Journal of Materials Chemistry A, 6 (2018) 1743-1750. https://doi.org/10.1039/c7ta09810c

[18] H.N. Wang, M. Zhang, A.M. Zhang, F.C. Shen, X.K. Wang, S.N. Sun, Y.J. Chen, Y.Q. Lan, Acs Applied Materials & Interfaces, 10 (2018) 32265-32270. https://doi.org/10.1021/acsami.8b12194

[19] S. Herrmann, N. Aydemir, F. Nagele, D. Fantauzzi, T. Jacob, J. Travas-Sejdic, C. Streb, Advanced Functional Materials, 27 (2017). https://doi.org/10.1002/adfm.201700881

[20] J. Vaillant, M. Lira-Cantu, K. Cuentas-Gallegos, N. Casañ-Pastor, P. Gómez-Romero,

Progress in Solid State Chemistry, 34 (2006) 147-159. https://doi.org/10.1016/j.progsolidstchem.2005.11.015
[21] M. Genovese, K. Lian, Electrochemistry Communications, 43 (2014) 60-62. https://doi.org/10.1016/j.elecom.2014.03.014
[22] A.K. Cuentas-Gallegos, R. Martínez-Rosales, M. Baibarac, P. Gómez-Romero, M.E. Rincón, Electrochemistry Communications, 9 (2007) 2088-2092. https://doi.org/10.1016/j.elecom.2007.06.003
[23] D.P. Dubal, P. Gomez-Romero, Materials Today Energy, 8 (2018) 109-117. https://doi.org/10.1016/j.mtener.2018.03.005
[24] M. Genovese, K. Lian, Journal of Materials Chemistry A, 5 (2017) 3939-3947. https://doi.org/10.1039/c6ta10382k
[25] C.C. Hu, E.B. Zhao, N. Nitta, A. Magasinski, G. Berdichevsky, G. Yushin, Journal of Power Sources, 326 (2016) 569-574. https://doi.org/10.1016/j.jpowsour.2016.04.036
[26] J. Suárez-Guevara, V. Ruiz, P. Gomez-Romero, Journal of Materials Chemistry A, 2 (2014) 1014-1021. https://doi.org/10.1039/c3ta14455k
[27] J. Suarez-Guevara, V. Ruiz, P. Gomez-Romero, Physical chemistry chemical physics : PCCP, 16 (2014) 20411-20414. https://doi.org/10.1039/c4cp03321c
[28] V. Ruiz, J. Suarez-Guevara, P. Gomez-Romero, Electrochemistry Communications, 24 (2012) 35-38. https://doi.org/10.1016/j.elecom.2012.08.003
[29] D.E. Jiang, Z. Jin, D. Henderson, J. Wu, The journal of physical chemistry letters, 3 (2012) 1727-1731. https://doi.org/10.1021/jz3004624
[30] L.L. Zhang, X.S. Zhao, Chem Soc Rev, 38 (2009) 2520-2531. https://doi.org/10.1039/b813846j
[31] D. Chai, Y. Hou, K.P. O'Halloran, H. Pang, H. Ma, G. Wang, X. Wang, ChemElectroChem, 5 (2018) 3443-3450. https://doi.org/10.1002/celc.201801081
[32] N.N. Du, L.G. Gong, L.Y. Fan, K. Yu, H. Luo, S.J. Pang, J.Q. Gao, Z.W. Zheng, J.H. Lv, B.B. Zhou, ACS Appl. Nano Mater., 2 (2019) 3039-3049. https://doi.org/10.1021/acsanm.9b00409
[33] K. Kume, N. Kawasaki, H. Wang, T. Yamada, H. Yoshikawa, K. Awaga, Journal of Materials Chemistry A, 2 (2014) 3801-3807. https://doi.org/10.1039/c3ta14569g
[34] L. Ouahab, M. Bencharif, A. Mhanni, D. Pelloquin, J. Halet, O. Pena, J. Padiou, D. Grandjean, C. Garrigou-Lagrange, Chemistry of materials, 4 (1992) 666-674. https://doi.org/10.1021/cm00021a032
[35] E. Bourgeat-Lami, F. Di Renzo, F. Fajula, P.H. Mutin, T. Des Courieres, The Journal of Physical Chemistry, 96 (1992) 3807-3811. https://doi.org/10.1021/j100188a044
[36] A.O. Kalpakli, S. Ilhan, C. Kahruman, I. Yusufoglu, International Journal of Refractory Metals and Hard Materials, 31 (2012) 14-20. https://doi.org/10.1016/j.ijrmhm.2011.08.007
[37] B. Chen, R. Neumann, Physical chemistry chemical physics : PCCP, 18 (2016) 22487-22493. https://doi.org/10.1039/c6cp03315f
[38] J. Cao, C. Li, Z. Zhang, C. Xu, J. Yan, F. Cui, C. Hu, J Am Soc Mass Spectrom, 23 (2012) 366-374. https://doi.org/10.1007/s13361-011-0296-4
[39] V.A. Grigoriev, C.L. Hill, I.A. Weinstock, Journal of the American Chemical Society, 122 (2000) 3544-3545. https://doi.org/10.1021/ja993862c
[40] T. Ueda, K. Kodani, H. Ota, M. Shiro, S.X. Guo, J.F. Boas, A.M. Bond, Inorg Chem, 56

(2017) 3990-4001. https://doi.org/10.1021/acs.inorgchem.6b03046
[41] Y.L. Shao, M.F. El-Kady, J.Y. Sun, Y.G. Li, Q.H. Zhang, M.F. Zhu, H.Z. Wang, B. Dunn, R.B. Kaner, Chemical Reviews, 118 (2018) 9233-9280. https://doi.org/10.1021/acs.chemrev.8b00252
[42] M. Zhang, A.M. Zhang, X.X. Wang, Q. Huang, X.S. Zhu, X.L. Wang, L.Z. Dong, S.L. Li, Y.Q. Lan, Journal of Materials Chemistry A, 6 (2018) 8735-8741. https://doi.org/10.1039/c8ta01062e
[43] S. Li, L.-L. Yu, R.-B. Li, J. Fan, J.-T. Zhao, Energy Storage Materials, 11 (2018) 176-183. https://doi.org/10.1016/j.ensm.2017.07.011
[44] X. Liu, C. Ma, J. Li, B. Zielinska, R.J. Kalenczuk, X. Chen, P.K. Chu, T. Tang, E. Mijowska, Journal of Power Sources, 412 (2019) 1-9. https://doi.org/10.1016/j.jpowsour.2018.11.032
[45] X. Yu, J. Lu, C. Zhan, R. Lv, Q. Liang, Z.-H. Huang, W. Shen, F. Kang, Electrochimica Acta, 182 (2015) 908-916. https://doi.org/10.1016/j.electacta.2015.10.016
[46] Q. Xie, R. Bao, A. Zheng, Y. Zhang, S. Wu, C. Xie, P. Zhao, ACS Sustainable Chemistry & Engineering, 4 (2016) 1422-1430. https://doi.org/10.1021/acssuschemeng.5b01417
[47] J. Niu, M. Liu, F. Xu, Z. Zhang, M. Dou, F. Wang, Carbon, 140 (2018) 664-672. https://doi.org/10.1016/j.carbon.2018.08.036
[48] J.Y. Hwang, M. Li, M.F. El-Kady, R.B. Kaner, Advanced Functional Materials, 27 (2017) 1605745. https://doi.org/10.1002/adfm.201605745
[49] Y. Wang, M. Zhang, Y. Dai, H.-Q. Wang, H. Zhang, Q. Wang, W. Hou, H. Yan, W. Li, J.-C. Zheng, Journal of Power Sources, 438 (2019) 227045. https://doi.org/10.1016/j.jpowsour.2019.227045
[50] J. Zhou, J. Lian, L. Hou, J. Zhang, H. Gou, M. Xia, Y. Zhao, T.A. Strobel, L. Tao, F. Gao, Nature communications, 6 (2015) 8503. https://doi.org/10.1038/ncomms9503
[51] J.-J. Zhu, L.-L. Yu, J.-T. Zhao, Journal of Power Sources, 270 (2014) 411-417. https://doi.org/10.1016/j.jpowsour.2014.07.093